

# 1 Search for Dark Matter Produced in Association with a 2 Hypothetical Dark Higgs Boson Decaying to $W^+W^-$ in 3 the $q\bar{q}\ell\nu$ Final State Using $pp$ Collisions Recorded with 4 the ATLAS Detector

Danika MacDonell

April 16, 2020

7 1 Introduction

8 The proposed thesis is a search for dark matter using high energy proton-proton ( $pp$ ) collision  
 9 data recorded with the ATLAS detector at the Large Hadron Collider (LHC). The search targets a  
 10 final state signature of dark matter production in association with the emission of a hypothetical  
 11 higgs boson  $s$  in the dark sector, which subsequently decays to a pair of W bosons. The search  
 12 is motivated by and optimized with a “dark higgs model” [1] shown in figure 2, in which the  $s$  is  
 13 emitted from a hypothetical  $Z'$  gauge boson in the dark sector, which itself mediates the production  
 14 of dark matter particles from the high energy  $pp$  collisions.

15 Any dark matter that may be produced in the  $pp$  collisions is expected not to interact to any  
 16 measurable extent with the ‘normal’ matter constituting the detector. As such, it is assumed that  
 17 the momentum carried by the dark matter would escape the detector undetected. However, the law  
 18 of momentum conservation requires that the momenta of all particles produced by a  $pp$  collision  
 19 in the plane transverse to the beam line sum to zero. This fundamental requirement implies that  
 20 dark matter produced at the LHC will exhibit a signature of high missing transverse momentum  
 21 in the final state. The magnitude of this two dimensional missing transverse momentum vector is  
 22 typically denoted “ $E_T^{\text{miss}}$ ”.

The aim of the proposed thesis work is to apply selections, including a requirement of high  $E_T^{\text{miss}}$ , to data from the ATLAS detector to optimize the sensitivity of the data to the dark higgs signal model. The data will subsequently be compared with standard model (SM) background and signal processes simulated with Monte Carlo (MC) to search for an above-background excess in the data consistent with the signal model.

28 The search is split into two separate analyses:

- 29    1. **The hadronic decay channel:** In this channel, each of the two W bosons in the final state  
 30    decay to quarks, which subsequently hadronize in the detector and are measured as jets in  
 31    the ATLAS calorimeter.

$$WW \rightarrow q\bar{q} + q\bar{q}$$

Given that the branching fraction for hadronic W decay is 0.68 [2], the fully hadronic WW decay occurs with a branching fraction of 0.46 ( $= 0.68^2$ ). In addition to its substantial branching fraction, this channel has the advantage of being able to fully reconstruct the momenta of both W bosons, and as such the  $s$  mass. The drawback is that there are standard model processes with large production cross section which also produce a final state of multiple jets in the detector, a subset of which pass the other signal selection criteria and represent a sizeable background in the analysis.

2. **The semileptonic decay channel:** One W boson decays to quarks in this channel, and the other decays to a lepton and a neutrino, where the lepton is either an electron or a muon.

$$WW \rightarrow q\bar{q} + \ell\nu$$

Despite its lower branching fraction of 0.29 [2] compared with the fully hadronic decay channel, the semileptonic channel has the advantage that the requirement of having one lepton in the final state reduces the background from standard model processes. However, this comes at the cost of additional  $E_T^{\text{miss}}$  from the neutrino production, which both inhibits reconstruction of the leptonically-decaying W boson and cannot easily be distinguished from the  $E_T^{\text{miss}}$  associated with dark matter production in the signal model.

There is an ongoing analysis searching for the dark higgs signal in the hadronic decay channel, and the proposed thesis will focus on the semileptonic decay channel.

The WW decay can also proceed via a fully leptonic channel, in which both W bosons decay to a lepton and a neutrino. This channel would give a clean signature of two leptons and no jets, but is currently not considered as a viable search channel due to its relatively low branching fraction of 0.046 [2].

Once the analysis is fully developed in the semileptonic decay channel, this channel will be statistically combined with the hadronic search channel. In the event that the combined search does not show an above-background excess, the analysis will place exclusion limits - to within some level of confidence, typically 95% - on the range of  $Z'$  and  $s$  masses in the dark higgs model to which the combined search is sensitive.

## 2 Motivation

The proposed thesis work would contribute to the extensive ongoing dark matter search program at the LHC. The LHC search program is motivated by compelling evidence from observational astronomy for the existence of dark matter constituting 85% [3] of all matter in the universe. Despite clear evidence from observational astronomy for its gravitational interactions with normal matter, dark matter has yet to be detected through the weak, strong or electromagnetic interactions. As such, its composition and non-gravitational interactions - if any - remain largely a mystery. The current most widely accepted and theoretically motivated dark matter candidates take the form of fundamental particles, yet there is no particle in the standard model of particle physics that could represent a viable dark matter candidate [4]. Dark matter is therefore widely assumed to be a “beyond-standard-model” (BSM) particle.

## 69 2.1 Dark Matter Search Methods

70 There are three complementary approaches used to search for particle dark matter: direct and  
 71 indirect detection, and collider searches. Direct detection searches [5, 6] aim to directly detect  
 72 evidence of a recoil induced by elastic scattering between a dark matter particle in the galactic  
 73 halo passing through the detector and a target particle in the detector. Indirect searches [7, 8]  
 74 use observational data to search for evidence of products produced by dark matter annihilation or  
 75 decay in particular regions of the observable universe expected to have a high dark matter density.  
 76 Collider searches [9], of which the proposed thesis work is an example, study the decay products  
 77 from high-energy collisions of subatomic particles to search for an above-background excess of  
 78 events that could be consistent with dark matter having been produced in some of the collisions.

## 79 2.2 Models of Dark Matter Production at Colliders

80 Models of dark matter production in colliders can range in complexity from an effective field the-  
 81 ory (EFT), where the dark matter production mechanism is completely unspecified, to a complete  
 82 model such as supersymmetry [10], which predicts viable dark matter candidates as part of a hy-  
 83 pothesized extension to the standard model designed to address a range of phenomena unexplained  
 84 by the standard model.

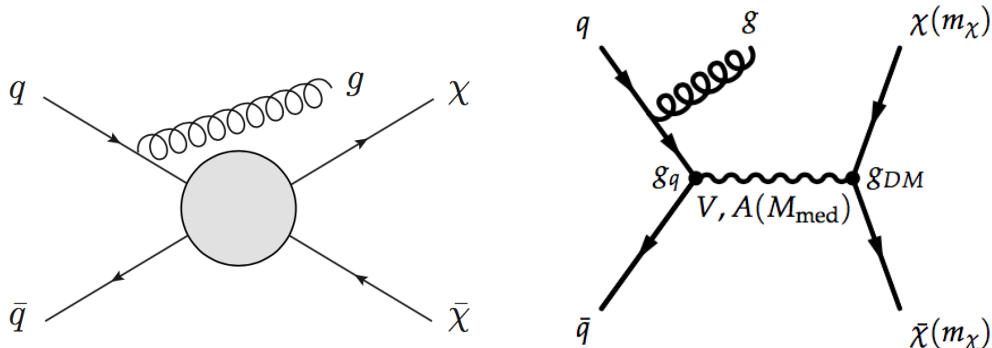


Figure 1: Left: Mono-jet process in the EFT framework (source: [11]). Right: Mono-jet process in a simplified model framework, where the pair production of dark matter occurs via a new vector or axial-vector ( $V, A$ ) mediator of mass  $M_{\text{med}}$ , which couples to quarks and dark matter with coupling constants  $g_q$  and  $g_{\text{DM}}$ , respectively (source: [12])

85 In principle, complete theories of physics beyond the standard model, such as the minimal  
 86 supersymmetric standard model (MSSM) [13] can offer theoretically motivated and experimentally  
 87 accessible models which specify the details of candidate processes by which the colliding partons  
 88 may annihilate to produce dark matter. However, these theories tend to be quite complex, with  
 89 many free parameters - over 100 in the case of MSSM [9] - most of which need to be fixed to  
 90 generate a reasonably testable model. Relying on complete theories alone to guide experimental  
 91 signatures may run the risk of missing important parameter space of new physics for which a  
 92 complete theory has not yet been developed.

93 Simplified models, widely used in recent and ongoing dark matter searches at the LHC, are  
 94 designed to bridge the gap between EFT and complete theories. They provide a ‘first-order’ de-

95 description of theoretically motivated new physics scenarios that could be accessible at collider ener-  
 96 gies. They provide guidance for experimental searches without fully specifying the details of any  
 97 additional new physics at energies above the collider scale that would be needed for a complete  
 98 theory [9]. In terms of dark matter production at the LHC, one or more new mediators associated  
 99 with new physics scenarios may be considered which allow for mixing between standard model  
 100 particles and dark matter. The process by which the mixing occurs is represented with a tree-level  
 101 diagram whose experimental signature would be accessible at LHC energies, such as the diagram  
 102 shown in figure 1 which represents a dark matter benchmark model featured in the 2015 report of  
 103 the ATLAS/CMS Dark Matter Forum [12].

### 104 **2.3 Dark Higgs Model**

105 The proposed search is motivated by and interpreted with a simplified model described in [1]  
 106 where dark matter is pair produced from a Z boson in the dark sector - known as the  $Z'$  boson - in  
 107 association with the emission of an additional dark sector higgs boson  $s$ . Figure 2 shows one of the  
 108 leading order Feynman diagrams representing this simplified model. The dark sector higgs boson  
 109 subsequently decays to a pair of massive standard model particles through a small mixing with the  
 110 SM higgs boson.

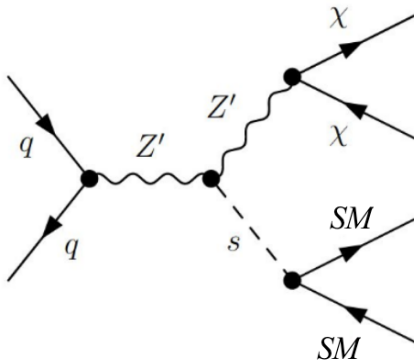


Figure 2: Dark higgs model

111 The generic hypothesis of ‘dark sector’ mediators which exhibit a small mixing with SM parti-  
 112 cles is motivated in part by the theoretical need for creation and annihilation mechanisms between  
 113 DM and SM particles in the well-motivated and popular ‘thermal freeze-out’ hypothesis [14]. In  
 114 the thermal freeze-out hypothesis, DM and SM particles interacted at a sufficient rate in the high  
 115 temperature and matter density of the early universe to remain in thermal equilibrium. Once the  
 116 DM-SM interaction rate dropped below the expansion rate of the universe, the DM rapidly “froze  
 117 out” of thermal equilibrium with the SM particles, at which point the relic abundance of DM was  
 118 fixed to the value observed in the present-day universe.

119 The dark higgs boson in particular is motivated by the need to generate the masses of dark  
 120 matter and any other particles residing in the dark sector [1]. If dark sector particle masses are  
 121 generated via a ‘dark sector higgs mechanism’, this would naturally imply the existence of a dark  
 122 higgs boson.

123        The model presented in [1] considers a scenario in which there is another dark sector mediator  
124 - taken to be the  $Z'$  - with a mass within the range accessible to measurement at the LHC, which  
125 mediates dark matter production from parton collisions. In this case, the  $Z'$  could radiate a dark  
126 higgs boson. Theoretically, the observed relic abundance of dark matter in the universe suggests  
127 that couplings between particles in the dark sector should be quite large, which could result in a  
128 sufficiently high probability of dark higgs emission from the  $Z'$  to produce a measurable signature  
129 in LHC collisions [1].

130        Experimentally, the dark higgs signature would be distinct from generic mono-X signatures  
131 where the SM particle that the dark matter recoils against is produced via initial state radiation,  
132 because as long as the combined mass of the  $Z'$  and  $s$  is well below the typical momentum transfer  
133 of the collisions, the  $s$  will tend to be highly boosted in the plane transverse to the beam line. As  
134 a result, the SM decay products will tend to be much higher in transverse momentum and highly  
135 collimated compared with particles produced via initial state radiation.

## 136        2.4 Experimental Background

137        This section discusses a previous experimental search which set exclusion limits on the dark higgs  
138 model described in Section 2.3, in the case where the dark higgs decays to a pair of b quarks.  
139 It goes on to describe the  $m_s$  range that the ongoing and proposed searches in the  $s \rightarrow WW$   
140 decay channel target, and explain how this target is complementary to the  $m_s$  range explored by  
141 the previous search in the  $s \rightarrow bb$  channel.

### 142        2.4.1 Re-interpretation of Mono-H(bb) Search with a Dark Higgs Mediator

143        Last year, the “mono-H(bb)” dark matter search, originally published in 2018 [15] with  $79.8 \text{ fb}^{-1}$   
144 of data taken with the ATLAS detector at a 13 TeV centre of mass energy, was re-interpreted [16]  
145 using the RECAST framework [17] to set exclusion limits on the dark higgs model in the case  
146 where the dark higgs decays to a pair of b-quarks.

147        The mono-H(bb) search selects for a final state of missing transverse energy along with two  
148 jets in the calorimeter, both of which must be tagged as having originated from the hadronization  
149 of b quarks. When the mono-H(bb) analysis was originally published, it had been developed  
150 and interpreted using a simplified model shown in figure 3 left, in which the dark matter is pair  
151 produced from a new pseudoscalar higgs boson, along with the emission of a SM higgs boson,  
152 which subsequently decays to two b quarks.

153        The original analysis was preserved using RECAST [17], a framework designed to preserve  
154 searches for new physics with high energy collision data in such a way that the searches can  
155 be readily re-analyzed with alternative models of new physics which predict the same final state  
156 signature. The RECAST framework was used to re-interpret the mono-H(bb) search using the  
157 dark higgs model shown in figure 3 right, where the dark higgs, whose mass is left as a floating  
158 parameter, decays to a pair of b quarks.

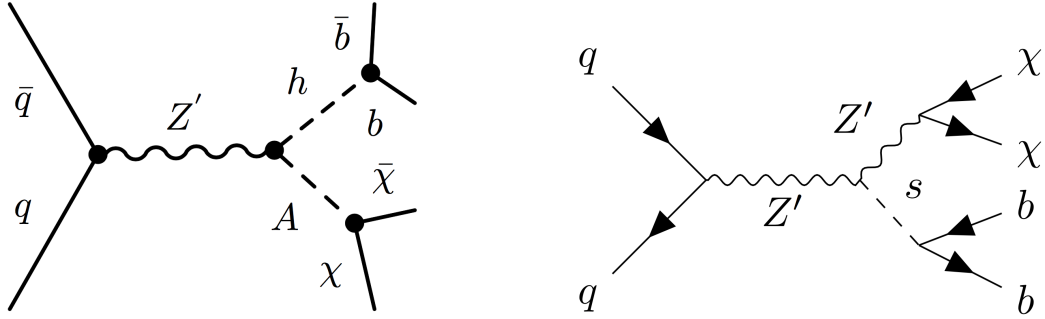


Figure 3: Left: Leading-order Feynman diagram representing the model used to interpret the mono-H(bb) dark matter search. Right: A leading-order Feynman diagram representing the model used to guide and interpret the mono-s(bb) re-interpretation of the mono-H(bb) search. The dark higgs mediator mass  $m_s$  is allowed to float in the dark higgs model.

159      The re-interpreted mono-H(bb) search set limits, shown in figure 4, on the phase space of  $Z'$   
 160     and  $s$  masses excluded by the data. To set these exclusion limits, several free parameters in the  
 161     dark higgs model need to be fixed. Specifically:

- 162     • The dark matter mass  $m_\chi$  is fixed to 200 GeV.
- 163     • The constant  $g_q$  associated with the coupling of the  $Z'$  boson to quarks is fixed to 0.25.
- 164     • The constant  $g_\chi$  associated with the coupling of the  $Z'$  boson to dark matter is fixed to 1.0.
- 165     • The mixing angle  $\theta$  between the dark and SM higgs bosons is fixed to 0.01.

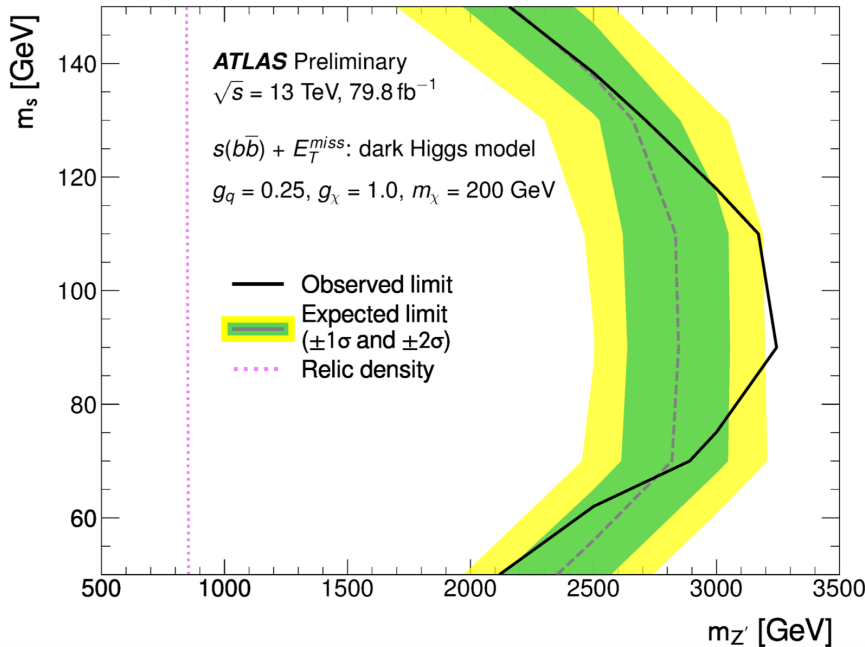


Figure 4: Exclusion limits set on the  $Z'$  and  $s$  mediator masses by the mono-H(bb) search re-interpreted with the dark higgs model. Mass combinations to the left of the solid black curve are excluded at a 95% confidence level. Source: [16]

166 The values of  $g_q$  and  $g_\chi$  were chosen to match the conventional choices used by other LHC DM  
 167 searches, and  $\theta$  matches the choice used in the original paper [1] that introduced the dark higgs  
 168 model.

#### 169 **2.4.2 Dark Higgs Decay Modes**

170 The re-interpreted mono-H(bb) search probed the dark higgs model in the case where the  $s$  emitted  
 171 from the  $Z'$  mediator decays to a pair of b quarks. However, predictions of the dark higgs branching  
 172 ratio presented in the re-interpretation paper [16] and shown in figure 5 indicate that the  $s \rightarrow bb$   
 173 decay mode is only sensitive to a range of dark higgs masses up to  $\sim 150$  GeV, above which the  
 174 WW decay mode dominates in sensitivity.

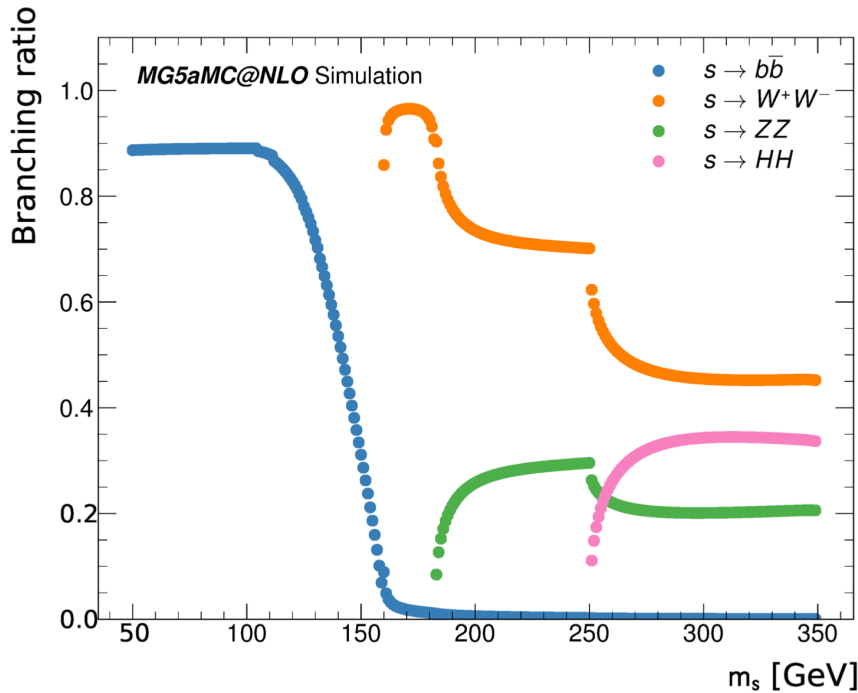


Figure 5: Predicted dark higgs decay branching ratios as a function of dark higgs mass. Source: [16]

175 There is no a-priori reason to expect the dark higgs mass  $m_s$  to necessarily lie below 150 GeV.  
 176 Therefore, it's important to probe the model in the higher  $m_s$  range by analyzing the  $s \rightarrow WW$   
 177 decay mode. The proposed thesis work will analyze the latter decay mode using the full  $139 \text{ fb}^{-1}$   
 178 ATLAS run 2 dataset, focusing on the semileptonic final state  $WW \rightarrow q\bar{q}\ell\nu$ .

### 179 3 Introduction to the LHC and the ATLAS detector

180 The Large Hadron Collider (LHC) [18] is a circular proton-proton collider which resides in a 27 km  
181 tunnel near the European Organization for Nuclear Research (CERN). Superconducting magnets  
182 are used to accelerate counter-rotating bunched proton beams to high energy, and direct the beams  
183 into head-on collisions at four interaction points around the ring. The collisions take place at a  
184 world-leading centre of mass energy of up to 13 TeV.

185 Each interaction point is surrounded by a detector, which measures the energetic debris of  
186 particles produced by the high energy collisions to perform precision measurements of the standard  
187 model and search for new physics. ATLAS (A Toroidal LHC ApparatuS) [19] is one of two multi-  
188 purpose detectors at the LHC, designed to record and study a wide range of physics processes  
189 resulting from the collisions.

190 The ATLAS detector, shown schematically in figure 6, provides full  $4\pi$  coverage around the  
191 interaction point, with the exception of the beam pipe. It consists of several layers of sub-detectors,  
192 each of which is specialized for recording certain kinematic information and particle types. The  
193 sub-detectors are described in some detail below.

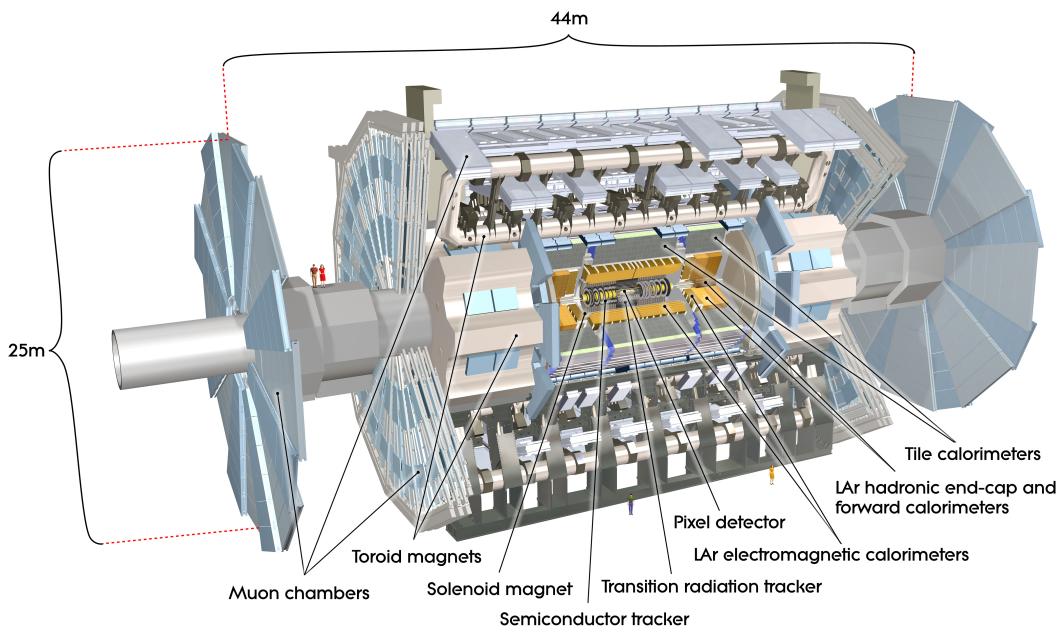


Figure 6: Schematic diagram of the ATLAS detector. Source: [19]

#### 194 3.1 The Inner Detector

195 The inner detector (ID), located nearest the the beam pipe, is specialized for charged particle  
196 tracking. It is immersed in a 2T magnetic field oriented parallel to the beam pipe, which bends  
197 the trajectories of electrically charged particles as they pass through the field. Three distinct but  
198 complementary tracking technologies are employed along with pattern recognition tools to map the  
199 trajectories of charged particles passing through the ID. These reconstructed tracks are a critical

200 component of vertex reconstruction, and the degree and direction of bent tracks provide information  
201 about the momentum, charge, and identity of the charged particles that produced them.

## 202 **3.2 The Calorimeter**

203 The calorimeter is designed to measure the energy of all particles which pass through it by initiating  
204 “showers” and fully absorbing their energy. The only particles which cannot be absorbed by the  
205 calorimeter are muons and neutrinos, which pass through without showering. The calorimeter is  
206 divided into two sub-detectors, the electromagnetic and hadronic calorimeters. Both are “sampling  
207 calorimeters”, which means they are comprised of repeated layers of dense absorbing material with  
208 “sampling” layers in between. The sampling layers track the location of the shower and record a  
209 small fraction of its energy, to which a calibration factor can be applied to infer the full shower  
210 energy.

### 211 **3.2.1 Electromagnetic Calorimeter**

212 The electromagnetic (EM) calorimeter forms the inner calorimeter layer, and is designed to fully  
213 absorb and measure the energy of electrons and photons. Energy is deposited in the iron-steel  
214 absorbing layers in the form of EM showers [20], in which the initial electron or photon interacts  
215 with the absorbing material to produce a cascade of photon radiation and electron pair production.  
216 The sampling layers are filled with liquid argon (LAr), with sensors to measure the ionization  
217 produced by charged particles passing through the LAr [21].

### 218 **3.2.2 Hadronic Calorimeter**

219 The hadronic calorimeter surrounds the EM calorimeter, and is designed to fully absorb and measure  
220 hadronic showers, also known as “jets”, initiated by hadrons, which can make it through the  
221 EM calorimeter due to their relatively long interaction length [19]. Unlike the EM showers de-  
222 scribed above which proceed exclusively via electromagnetic interactions, hadronic showers pro-  
223 ceed via both the strong and EM interactions, and as a result are in general more variable and less  
224 localized.

225 The hadronic calorimeter is comprised of a tile calorimeter which encircles the EM calorimeter  
226 barrel, and a LAr calorimeter with copper and tungsten absorbers in the end-cap region which  
227 encloses the two ends of the barrel. The tile calorimeter uses steel as the absorber material and  
228 scintillators read out by photomultiplier tubes (PMTs) in the sampling layers.

## 229 **3.3 The Muon Spectrometer**

230 The muon spectrometer [19] surrounding the calorimeter is specialized for tracking muons and  
231 measuring their momentum. It employs the same principle used in the inner detector of applying  
232 a strong magnetic field and measuring the resulting bent tracks of the electrically charged muons  
233 passing through to infer their momentum.

234 The magnetic field is generated by rectangular superconducting “toroid magnets” arranged  
235 radially around the beam axis, which set up a toroidal field concentric to the beam axis. In the  
236 region containing the strong field established by the toroid magnets, muon tracks are recorded

<sup>237</sup> by three cylindrical layers of muon tracking chambers in the barrel region and three layers of  
<sup>238</sup> chambers arranged in wheels perpendicular to the beam axis in the end-cap region. Additional  
<sup>239</sup> layers of fast trigger chambers deliver muon track information to the ATLAS trigger system so it  
<sup>240</sup> can be incorporated into the event readout decision.

241 **4 Ongoing analysis of mono-s(WW) hadronic channel**

- 242     • Preselection  
 243     • Signal region selection  
 244     • Control regions  
 245     • Very brief summary of systematics (exp and modeling)  
 246     • Sensitivity estimates  
 247     • RECAST

248 **5 Signal Sample Generation for Semileptonic Channel**

249 The mass of a dark matter particle is fixed to  $200 \text{ GeV}/c^2$ , and the  $Z'$  and dark higgs masses are  
 250 allowed to vary from  $500 \text{ GeV}/c^2$  to  $2500 \text{ GeV}/c^2$  and  $160 \text{ GeV}/c^2$  to  $360 \text{ GeV}/c^2$ , respectively.

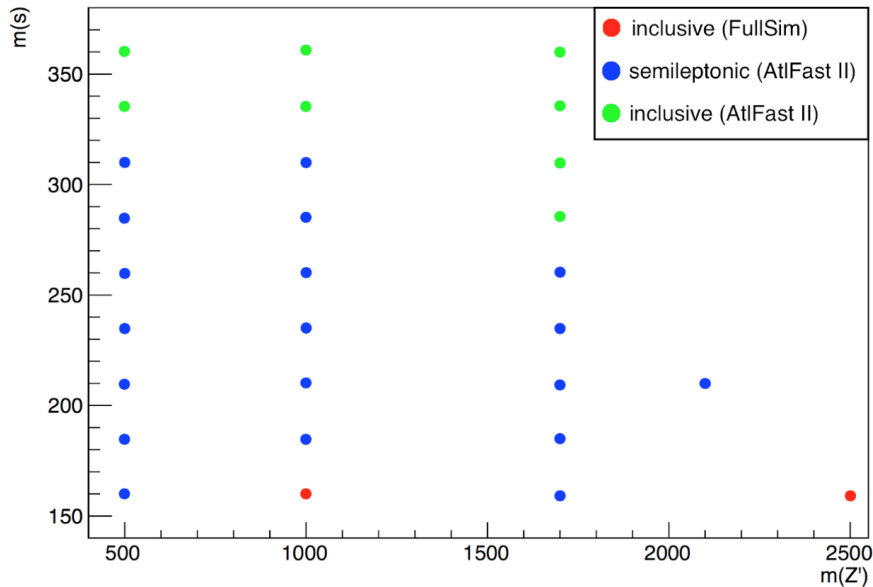


Figure 7: Grid of signal points with respect to dark higgs ( $s$ ) and  $Z'$  boson masses of generated signal sample

- 251     • Scan over range of  $m(s)$  and  $m(Z')$   
 252     • Need to fix some parameters in the model:  
 253        –  $g_q = 0.25$   
 254        –  $g_\chi = 1$   
 255        –  $\theta = 0.01$

256        -  $m_\chi = 200$  GeV

- 257        • Discuss motivation for above choices of fixed model parameters

## 258    6 Event Selection for Semileptonic Channel

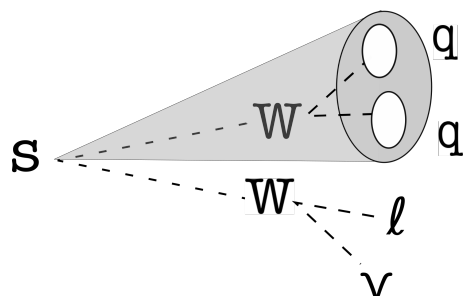
### 259    6.1 Preselection

- 260        • MET trigger passed  
261        • 1 signal lepton  
262        • MET  $\gtrsim 150$  GeV

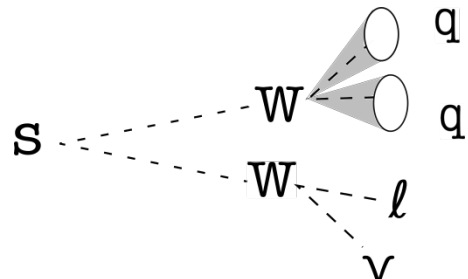
### 263    6.2 Regions

- 264        • Signal region  
265        • W+jets control region  
266        • ttbar control region (if we plan to do one)

### 267    6.3 Categories



(a) Merged category



(b) Resolved category

Figure 8: Kinematic categories for final state selection

- 268        • Resolved category  
269        • Merged category

270 **7 Sensitivity Studies**

271 **7.1 Background on limit setting**

272 **7.2 HistFitter setup**

- 273 • Fit variable

- 274 • Binning

- 275 • Use of temporary systematics proxy

276 **7.3 Preliminary sensitivity limits**

- 277 • Resolved

- 278 • Merged

- 279 • Combined

280 **8 Remaining Work and Outlook**

- 281 • Study variables to help address  $p_\nu$  vs.  $p_{\chi\bar{\chi}}$  MET ambiguity

- 282 • Finalize SR and CR definitions

- 283 • Experimental and modeling systematics

- 284 • Finalize sensitivity estimates with final systematics

- 285 • Statistical combination with hadronic channel for combined limits

286 **References**

- 287 [1] Michael Duerr, Alexander Grohsjean, Felix Kahlhoefer, Bjoern Penning, Kai Schmidt-  
288 Hoberg, and Christian Schwanenberger. Hunting the dark higgs. *Journal of High Energy*  
289 *Physics*, 2017(4), Apr 2017.
- 290 [2] M. Tanabashi et al. (Particle Data Group), Phys. Rev. D 98, 030001 (2018) and 2019 update.
- 291 [3] N. et al. Aghanim. Planck 2018 results. VI. Cosmological parameters. 7 2018.
- 292 [4] J. L. Feng. Dark matter candidates from particle physics and methods of detection. *Annual*  
293 *Review of Astronomy and Astrophysics*, 1(48):495–545, 2010.
- 294 [5] Marc Schumann. Direct detection of WIMP dark matter: concepts and status. *Journal of*  
295 *Physics G: Nuclear and Particle Physics*, 46(10):103003, aug 2019.
- 296 [6] Teresa Marrodan Undagoitia and Ludwig Rauch. Dark matter direct-detection experiments.  
297 *J. Phys. G*, 43(1):013001, 2016.
- 298 [7] Marco Cirelli. Indirect searches for dark matter. *Pramana*, 79(5):1021–1043, Oct 2012.
- 299 [8] Jan Conrad and Olaf Reimer. Indirect dark matter searches in gamma- and cosmic rays.  
300 *Nature Physics*, 13:224–231, 03 2017.
- 301 [9] Antonio Boveia and Caterina Doglioni. Dark matter searches at colliders. *Annual Review of*  
302 *Nuclear and Particle Science*, 68(1):429–459, 2018.
- 303 [10] Gerard Jungman, Marc Kamionkowski, and Kim Griest. Supersymmetric dark matter. *Phys.*  
304 *Rept.*, 267:195–373, 1996.
- 305 [11] O. Buchmueller, Matthew J. Dolan, and Christopher McCabe. Beyond Effective Field Theory  
306 for Dark Matter Searches at the LHC. *JHEP*, 01:025, 2014.
- 307 [12] Daniel Abercrombie, Nural Akchurin, Ece Akilli, Juan Alcaraz Maestre, Brandon Allen, Bar-  
308 bara Alvarez Gonzalez, Jeremy Andrea, Alexandre Arbey, Georges Azuelos, Patrizia Azzi,  
309 and et al. Dark matter benchmark models for early lhc run-2 searches: Report of the atlas/cms  
310 dark matter forum. *Physics of the Dark Universe*, 27:100371, Jan 2020.
- 311 [13] Csaba Csaki. The minimal supersymmetric standard model (mssm). *Modern Physics Letters*  
312 *A*, 11(08):599–613, Mar 1996.
- 313 [14] Stefano Profumo, Leonardo Giani, and Oliver F. Piattella. An introduction to particle dark  
314 matter, 2019.
- 315 [15] Search for Dark Matter Produced in Association with a Higgs Boson decaying to  $b\bar{b}$  at  $\sqrt{s} =$   
316 13 TeV with the ATLAS Detector using  $79.8 \text{ fb}^{-1}$  of proton-proton collision data. Technical  
317 Report ATLAS-CONF-2018-039, CERN, Geneva, Jul 2018.

- 318 [16] RECAST framework reinterpretation of an ATLAS Dark Matter Search constraining a model  
319 of a dark Higgs boson decaying to two  $b$ -quarks. Technical Report ATL-PHYS-PUB-2019-  
320 032, CERN, Geneva, Aug 2019.
- 321 [17] Kyle Cranmer and Itay Yavin. Recast - extending the impact of existing analyses. *Journal of*  
322 *High Energy Physics*, 2011(4), Apr 2011.
- 323 [18] Lyndon Evans and Philip Bryant. LHC machine. *Journal of Instrumentation*, 3(08):S08001–  
324 S08001, aug 2008.
- 325 [19] G. Aad et al. The ATLAS Experiment at the CERN Large Hadron Collider. *JINST*, 3:S08003,  
326 2008.
- 327 [20] Lev Davydovitch Landau, G. Rumer, and Piotr Leonidovich Kapitza. The cascade theory of  
328 electronic showers. *Proceedings of the Royal Society of London. Series A. Mathematical and*  
329 *Physical Sciences*, 166(925):213–228, 1938.
- 330 [21] Huaqiao Zhang and. The ATLAS liquid argon calorimeter: Overview and performance.  
331 *Journal of Physics: Conference Series*, 293:012044, apr 2011.